Photoconductivity and highly selective ultraviolet sensing features of amorphous silicon carbon nitride thin films

Chun-Wei Chen,[a] Cheng-Chia Huang, Yun-Yue Lin, and Wei-Fang Su
Department of Materials Science and Engineering, National Taiwan University, Taipei, Taiwan

Li-Chyong Chen[b]
Center for Condensed Matter Sciences, National Taiwan University, Taipei, Taiwan

Kuei-Hsien Chen
Institute of Atomic and Molecular Sciences, Academic Sinica, Taipei, Taiwan

(Received 9 August 2005; accepted 10 January 2006; published online 17 February 2006)

Photoconductivity of amorphous silicon carbon nitride (*a*-SiCN) as a function of incident photon energies has been studied. A metal-semiconductor-metal photodetector device based on the *a*-SiCN thin film demonstrates excellent selective ultraviolet sensing features. A large photo-to-dark current ratio about 5000 and a relative quantum efficiency about $\sim 10^5$ under illumination of the 250 nm light source and a bias voltage of 5 V were observed. A model based on the heterogeneous structure in the *a*-SiCN thin film which consists of $\pi-\pi^*$ bands and $\sigma-\sigma^*$ bands was introduced to account for the observed photoconductive transport properties. © *2006 American Institute of Physics*. [DOI: 10.1063/1.2178406]

Recently, a class of ternary silicon carbon nitride (SiCN) materials with large (several tens of microns) and well-faceted crystals has been grown by microwave plasma-enhanced chemical vapor deposition (MW-CVD).[1–3] Composition and bonding analyses suggest the structure of SiCN to be a solid solution of SiN_x and CN_x, in that C atoms substitute only for the Si sites and vice versa. The optical investigation of polycrystalline SiCN films with a Si to C ratio near 1 showed a direct band gap of about 3.8 eV.[2] Moreover, it was shown that optical properties in the *a*-SiCN thin films such as transmittance, index of refraction (2.0–2.2) and optical band gap (4.1–3.3 eV) can be tuned by varying the carbon content from 0 to 25%.[4] Thus Si_xC_yN constitutes an important wide-band-gap material with band-gap energy within the blue-ultraviolet (UV) spectral region. Concerning the nature of high thermal stability and wide band gap in amorphous silicon carbon nitride (*a*-SiCN) thin films, it is expected that the material could offer much promise in the development for UV detection. In this letter, we present a study on the photoconductivity and transport mechanism of the *a*-SiCN thin film based on a metal-semiconductor-metal (MSM) photodetector device. The photosensitivity and the relative quantum efficiencies (RQE) as a function of incident photon energy were measured to investigate its potential application for UV light detection. Finally, a model based on the electronic density of states (DOS) is proposed to explain the transport properties from different recombination mechanisms.

A MW-CVD (AsTex, 5 kW) technique was employed to grow the SiCN films on a Si(100) *p*-type substrate. The starting gas pressure was controlled by throttle valve at about 28 mTorr during deposition. A microwave power of 1.5 kW was set to generate plasma with a mixture of semiconductor grade SiH_4 (3 sccm), NH_3 (30 sccm), CH_4 (30 sccm), and H_2 (100 sccm) gases, respectively. The chemical compositions and bonding states of the *a*-SiCN thin films were determined by x-ray photoelectron spectroscopy (XPS) (Perkin–Elmer Phi 1600). The photovoltaic device with an MSM structure was then fabricated by depositing the 900 nm thick *a*-SiCN film on the silicon (100) substrate and evaporating the Au on top to form the electrode. The sample area is 0.25 cm^2 for the device. A light source from a 300 W xenon lamp (Oriel) was used to irradiate the device with a monochromatic light. Photocurrent measurements were completed using a Keithley 6487 source measurement unit to monitor the current and voltage. For comparison, an MSM device with the same structure based on the *a*-Si_3N_4 thin film was also fabricated. The optical band gap for the *a*-Si_3N_4 thin film is about 4.8 eV.

High-resolution XPS scans of Si(2*p*), C(1*s*), and N(1*s*) peaks of the *a*-SiCN thin film were performed to obtain the chemical composition and bonding configuration of the *a*-SiCN network. The deposited *a*-SiCN thin film has the chemical composition of Si(35%):C(24%):N(39%):O(2%) and the deconvoluted Si(2*p*), C(1*s*), and N(1*s*) bands were shown in Figs. 1(a)–1(c), respectively. In the Si(2*p*) spectrum, the predominant Si–N signature (102 eV) is found, and there is no major peak that matches the Si–C binding energy at 100.3 eV, indicating the negligible presence of Si–C bonds in the *a*-SiCN thin films as suggested before.[5] Figure 1(b) depicts the 285.9 and 287.3 peaks corresponding to $C(sp^2)-N$ and $C(sp^3)-N$ bonds, respectively.[6–9] The contributions at 397.6, 398.7, and 399.9 eV are related to the N–Si, $N-C(sp^3)$, and $N-C(sp^2)$, respectively.[10,11] In addition, it was found (not shown here) that the *a*-SiCN thin films with different carbon content exhibited similar signatures in the XPS spectra but showed the variation of the area ratio of $C(sp^3)-N/C(sp^2)-N$ or $N-C(sp^3)/N-C(sp^2)$ in the C(1*s*) or N(1*s*) spectra. Predominantly sp^3-bonded C–N sites were found in the *a*-SiCN thin films with a lower carbon content, while the enhancement of sp^2-bonded $C(sp^2)-N$ sites appeared with the increase of carbon content.

[a]Electronic mail: chunwei@ntu.edu.tw
[b]Electronic mail: chenlc@ntu.edu.tw

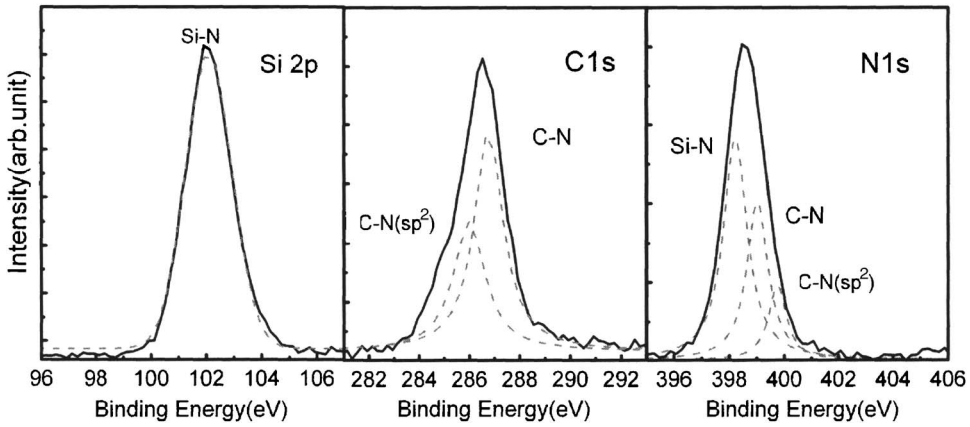

FIG. 1. XPS spectra of (a) Si(2*p*), (b) C(1*s*), and (c) N(1*s*) for the *a*-SiCN thin film with the composition of Si(35%):C(24%):N(39%):O(2%).

Figure 2 shows the characteristics of photocurrent-voltage response of the Au/*a*-SiCN/Si MSM photovoltaic device under the irradiation of light with various wavelengths. It is clearly shown that the photoconductive current of the Au/*a*-SiCN/Si device increases dramatically for the illuminating light with a wavelength shorter than 350 nm, indicating that the device possesses a selective sensing feature of good deep-UV detection ability. The inset shows the spectral response of photosensitivity *S*, defined as the photocurrent I_p to dark current I_d ratio I_p/I_d with an applied voltage of 5 V. The *S* reaches a value of about 5000 for the incident light with a wavelength of 250 nm, which is much higher than those reported prior to this study.[12] The Au/*a*-Si_3N_4/Si device investigated for comparison under the same experimental conditions showed no enhancement of current for incident light with wavelength from 250 to 700 nm, indicating the highly insulating properties of *a*-Si_3N_4.

By normalizing the incident Xe light spectra, the spectral response of the RQE for the Au/*a*-SiCN/Si device is shown in Fig. 3(a). These values were obtained by taking the quantum efficiency as 1 for the sample under the illuminated light with a wavelength 250 nm. A ratio of about $\sim 10^5$ can be achieved for the illuminating light with a wavelength of

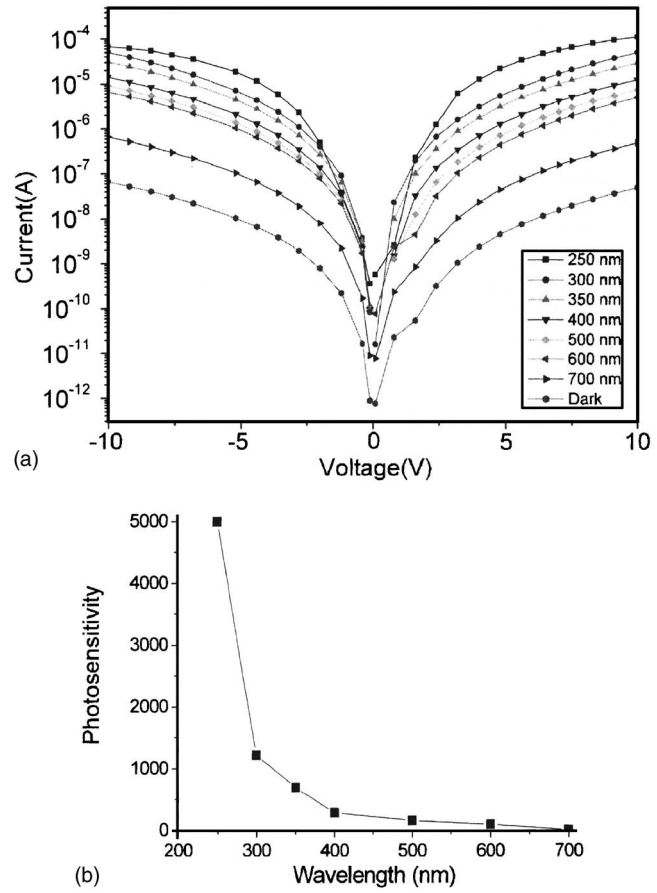

FIG. 2. (a) Characteristics of photocurrent-voltage response of the Au/*a*-SiCN/Si MSM photodetector device under the irradiation of light sources with various wavelengths. (b) The spectral response of photosensitivity *S* under an applied voltage of 5 V. The incident light intensities from the monochromatic Xe light source are 0.06 (250 nm), 0.37 (300 nm), 0.30 (350 nm), 0.61 (400 nm), 0.84 (500 nm), 0.71 (600 nm), and 1.04 (700 nm) mW/cm^2, respectively.

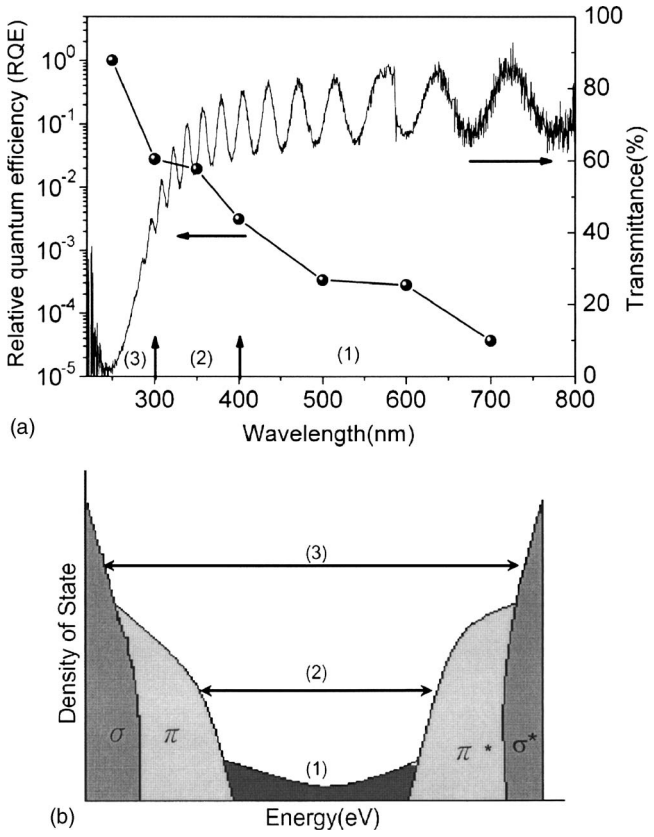

FIG. 3. (a) Spectral response of the RQE. The quantum efficiency for the sample under the illuminated light with a wavelength 250 nm is taken as 1. The corresponding optical transmittance of *a*-SiCN thin film is also shown. (b) Schematic models of the (1) defect band, the (2) localized $\pi-\pi^*$ bands, and the (3) extended $\sigma-\sigma^*$ bands, respectively, in the *a*-SiCN thin films. Regions (1), (2), and (3) have the same descriptions as in (a) and (b).

250 nm, compared to that with a wavelength of 700 nm. The corresponding transmission spectrum for the *a*-SiCN thin film is also shown. Transmittance measurements were used to determine the optical absorption energy gap of E_{opt}, following the Tauc's relation for amorphous materials.[13] The resulting optical absorption gap E_{opt} is about 3.2 eV (400 nm). The observed gradual change of the RQE in the vicinity of the optical absorption gap E_{opt} is attributed to the band tail broadening in typical amorphous materials (Ubach tail).

A model based on the electronic DOS of *a*-SiCN is proposed to explain the observed highly selective UV sensing features. As shown in the XPS spectra in Fig. 1, carbon and nitrogen in *a*-SiCN possess a wide range of bonding configurations, giving a heterogeneous structure which consists of $\pi-\pi^*$ bands and σ-σ^* bands. The appearance of C(sp^2)–N sites introduces the localized $\pi-\pi^*$ bands within the predominantly sp^3-bonded C–N and Si–N matrix. Figure 3(b) shows the schematic locations of the (1) defect band, the (2) localized $\pi-\pi^*$ bands, and the (3) extended $\sigma-\sigma^*$ bands, respectively. The defect band and the localized $\pi-\pi^*$ bands act as the deep traps and shallow traps, corresponding to the defective and absorption edge regions respectively. Electrons and holes recombine through the defective states, which are predominantly nonradiative. The defect band [Region (1)] originates from the disorder and dangling bonds in the *a*-SiCN network. The considerably low quantum efficiency for the incident light with a wavelength of 700 nm is mainly attributed to the defective midgap states in Region (1). The π bonding valence band and π^* antibonding conduction band result from the existence of C(sp^2)–N sites in the *a*-SiCN thin film. In addition, a nitrogen lone pair state is also believed to form in the π valence band.[14] The optical absorption edge resulting from the $\pi-\pi^*$ transition is about 3.2 eV (400 nm) corresponding to the transition in Region (2). The substitution of carbon atoms for Si sites in the SiCN network not only lowers the band gap due to its higher covalent features of C–N than Si–N (Ref. 14) but also promotes the formation of C(sp^2)–N sites as mentioned above. These lead to the higher dark current in the *a*-SiCN MSM device compared to the *a*-Si_3N_4 counterpart. The localized $\pi-\pi^*$ bands consist of shallow traps, from which the carriers are usually thermally excited back to the conduction band edge. This accounts for the further increase of photocurrent for the incident light with the photon energy larger than the E_{opt} (3.2 eV) in Region (2). Due to the nature of highly localized $\pi-\pi^*$ bonding features in the tail states,[15] the $\pi-\pi^*$ bands have less contributions on photoconductivity than the $\sigma-\sigma^*$ bands ?because of the small capture radius in the $\pi-\pi^*$ bands as seen in *a*-C.[16] The σ bonding valence band and the σ^* antibonding conduction band shown in Region (3) correspond to the highly photoconductive region. In this region, the energy gap >4.1 eV (300 nm) represents the mobility gap above which the photogenerated carriers can move freely and contribute to a large photoconductive current and a dramatic increase in the RQE. The correlation between Figs. 3(a) and 3(b) gives the evidence that optical absorption gap lies within the mobility gap. The large difference in the RQE between Regions (1) and (3) indicates the excellent selective UV sensing properties of the *a*-SiCN thin film.

In conclusion, photoconductive properties of the *a*-SiCN thin film have been investigated. The simple Au/*a*-SiCN/Si MSM device demonstrates excellent selective UV sensing features. Combined with the excellent thermal stability and the ability for band gap engineering, the *a*-SiCN based MSM device can be further developed into the potential applications of low-cost UV photodetectors.

This work is supported by National Science Council, Taiwan (Project Nos. NSC 93-2120-M-002-010 and NSC 93-2112-M-002-031).

[1] L. C. Chen, C. Y. Yang, D. M. Bhusari, K. H. Chen, M. C. Lin, J. C. Lin, and T. J. Chung, Diamond Relat. Mater. **5**, 514 (1996).
[2] L. C. Chen, C. K. Chen, S. L. Wei, D. M. Bhusari, K. H. Chen, Y. F. Chen, Y. C. Jong, and Y. S. Hunag, Appl. Phys. Lett. **72**, 2463 (1998).
[3] A. Badzian and T. Badzian, Diamond Relat. Mater. **7**, 1519 (1998).
[4] C. W. Chen, C. C. Huang, Y. Y. Lin, L. C. Chen, K. H. Chen, and W. F. Su, Diamond Relat. Mater. **14**, 1010 (2005).
[5] C. W. Chen, C. C. Huang, Y. Y. Lin, L. C. Chen, and K. H. Chen, Diamond Relat. Mater. **14**, 1126 (2005).
[6] D. Marton, K. J. Boyd, A. H. Al-Bayati, S. S. Todorov, and J. W. Rabalais, Phys. Rev. Lett. **73**, 118 (1994).
[7] J. P. Zhao, Z. Y. Chen, T. Yano, T. Ooie, M. Yoneda, and J. Sakakibara, J. Appl. Phys. **89**, 1643 (2001).
[8] S. Bhattacharyya, C. Cardinaud, and G. Turban, J. Appl. Phys. **83**, 4991 (1998).
[9] B. C. Holloway, O. Kraft, D. K. Shuh, M. A. Kelly, W. D. Nix, P. Pianetta, and S. Hagström, Appl. Phys. Lett. **74**, 3290 (1999).
[10] G. Lehmann, P. Hess, J.-J. Wu, C. T. Wu, T. S. Wong, K. H. Chen, L. C. Chen, H.-Y. Lee, M. Amkreutz, and T. Frauenheim, Phys. Rev. B **64**, 165305 (2001).
[11] J. M. Ripalda, L. Galán, and I. Montero, Diamond Relat. Mater. **7**, 402 (1996).
[12] W. R. Chang, Y. K. Fang, S. F. Ting, Y. S. Tsair, C. N. Chang, C. Y. Lin, and S. F. Chen, IEEE Electron Device Lett. **24**, 565 (2003).
[13] J. Tauc, R. Grigorovici, and A. Vancu, Phys. Status Solidi **15**, 627 (1969).
[14] C. W. Chen, M. H. Lee, L. C. Chen, and K. H. Chen, Diamond Relat. Mater. **13**, 1158 (2004).
[15] C. W. Chen and J. Robertson, J. Non-Cryst. Solids **227**, 602 (1998).
[16] A. Ilie, O. Harel, N. M. J. Conway, T. Yagi, J. Robertson, and W. I. Milne, J. Appl. Phys. **87**, 789 (2000).